APL MATERIALS **3**, 106102 (2015)

# Crystallization engineering as a route to epitaxial strain control

Andrew R. Akbashev,[1] Aleksandr V. Plokhikh,[1] Dmitri Barbash,[1]
Samuel E. Lofland,[2] and Jonathan E. Spanier[1,3,a]
[1]*Department of Materials Science and Engineering, Drexel University, Philadelphia, Pennsylvania 19104, USA*
[2]*Department of Physics, Rowan University, Glassboro, New Jersey 08028, USA*
[3]*Department of Physics, Drexel University, Philadelphia, Pennsylvania 19104, USA*

(Received 10 July 2015; accepted 30 September 2015; published online 16 October 2015)

The controlled synthesis of epitaxial thin films offers opportunities for tuning their functional properties via enabling or suppressing strain relaxation. Examining differences in the epitaxial crystallization of amorphous oxide films, we report on an alternate, low-temperature route for strain engineering. Thin films of amorphous Bi–Fe–O were grown on (001)$SrTiO_3$ and (001)$LaAlO_3$ substrates via atomic layer deposition. *In situ* X-ray diffraction and X-ray photoelectron spectroscopy studies of the crystallization of the amorphous films into the epitaxial (001)$BiFeO_3$ phase reveal distinct evolution profiles of crystallinity with temperature. While growth on (001)$SrTiO_3$ results in a coherently strained film, the same films obtained on (001)$LaAlO_3$ showed an unstrained, dislocation-rich interface, with an even lower temperature onset of the perovskite phase crystallization than in the case of (001)$SrTiO_3$. Our results demonstrate how the strain control in an epitaxial film can be accomplished via its crystallization from the amorphous state.  [http://dx.doi.org/10.1063/1.4933064]

The importance of the strain engineering for the control of the properties of epitaxial thin films has been highlighted by various strain-induced phenomena such as the ferroelectricity in $SrTiO_3$,[1] accelerated oxygen exchange at the surface of $Nd_2NiO_{4+\delta}$,[2] enhanced ferroelectric transition temperature in $BaTiO_3$,[3] realization of strong ferroelectric and ferromagnetic properties in $EuTiO_3$ thin films,[4] and magnetic phase segregation in $La_{2/3}Ca_{1/3}MnO_3$ thin films.[5] The growth of epitaxially strained or relaxed thin films with reasonable lattice matching can be accomplished via different routes, but in every case, it requires certain growth parameters and the procedure to be followed. However, one of the key aspects of such approaches is the formation of the strained/relaxed film directly during growth, which typically requires high temperatures and high or ultra-high vacuum.[6,7] A different approach has been proposed,[8] which is based on the low-temperature atomic layer deposition of the amorphous *A*–*B*–O film followed by its *ex situ* crystallization into the epitaxial perovskite $ABO_3$ on the lattice-matched substrate. The control of the epitaxial crystallization of such films offers a new pathway towards manipulating their strain state and, hence, functional properties.

Here, we choose $BiFeO_3$ as a model perovskite material, the epitaxial thin films of which have been well studied and can be grown using various techniques such as physical vapor deposition (e.g., pulsed laser deposition, PLD,[9] and RF sputtering[10]), metal-organic chemical vapor deposition (MOCVD),[11,12] and molecular beam epitaxy.[13] Co-existence of both ferroelectric and magnetic ordering makes $BiFeO_3$ one of the most intriguing electronic materials. Coupled with its large electromechanical response, a visible-wavelength bandgap and thickness- and strain-engineered ferroelectric domain structure, $BiFeO_3$, and its solid solutions continue to attract attention for

[a]Email: spanier@drexel.edu

 

potential applications in multiferroic, multi-state, tunneling electroresistive and optical memories, and ferroelectric photovoltaics.[14,15]

In this study, we report on the epitaxial crystallization of Bi–Fe–O thin films grown by atomic layer deposition (ALD) on single-crystal (001)$LaAlO_3$ and (001)$SrTiO_3$ substrates. When grown on (001)$LaAlO_3$ by PLD, due to a high lattice mismatch and corresponding epitaxial strain, $BiFeO_3$ becomes tetragonal and exhibits a different ferroelectric behavior than its rhombohedral modification.[16] In our case, however, we show that epitaxial $BiFeO_3$ films produced by ALD and subsequent annealing on (001)$LaAlO_3$ exhibit a strain relaxation and periodic misfit dislocations not present in epitaxial films formed by higher temperature methods, where crystallization occurs during deposition. Because in the ALD experiments, Bi–Fe–O thin films are grown from metal-organic precursors, they typically contain carbon atoms as impurity species. Such carbon impurities negatively affect the overall dielectric and, consequently, ferroelectric performance of oxides, increasing leakage currents[17] and introducing charge-trapping centers.[18] Here, we also investigate the evolution of carbon residuals *in situ* during annealing in the X-ray photoelectron spectrometer. The control of carbon impurities is essential for attaining the desired ferroelectric and dielectric properties of ALD-grown ferroelectric oxides.

Atomic layer deposition of Bi–Fe–O thin films was carried out with an ALD reactor (Cambridge Nanotech Savannah 100) on single-crystalline $SrTiO_3$ and $LaAlO_3$ substrates (MTI Corporation). Substrates were placed ~3-4 cm from the gas inlet and the chamber was held at 200 °C during growth. Ferrocene ($Fe(cp)_2$, Sigma-Aldrich F408) and $Bi(mmp)_3$ (tris(1-methoxy-2-methyl-2-propoxy)bismuth, Sigma-Aldrich American Elements, PN: BI-OMX-03M-C, 99.9% purity)) were heated to 90 °C and 135-145 °C, respectively, and used as volatile precursors. Oxidation of each precursor layer was carried out using ozone ($O_3$). For Bi–Fe–O films, the pulse ratio between the metal precursors was $Bi(mmp)_3$:$Fe(cp)_2$ = $n$:$m$, where $n$ = 2 or 3 and 12 < $m$ < 22. The thickness of the films varied from 25 to 50 nm.

X-ray diffraction was performed in a 4-circle X-ray diffractometer (Rigaku Smartlab, 40 kV, 44 mA, Cu K$\alpha$) equipped with a double (220)Ge monochromator in a parallel beam geometry. Reciprocal space mapping was carried out in a separate diffractometer (Panalytical Empyrean, double (220)Ge monochromator, 45 kV, 40 mA) for each of the (103) peaks of the perovskite substrates and the films. A 1/32° divergence slit was used for $BiFeO_3$/$SrTiO_3$ and 1/2° for $BiFeO_3$/$LaAlO_3$. Annealing of the stoichiometric films on $SrTiO_3$, on $LaAlO_3$, and on YSZ was conducted in a commercial domed hot stage (Anton Paar DHS 1100) in vacuum ($10^{-1}$ mbar) at temperatures up to 700 °C.

*In situ* XRD measurements were carried out with a temperature step of 25 °C and 40 min of the total measurement time at each temperature point (heating rate was ~5 °C/min). Specimen preparation for TEM was performed with a dual-beam focused ion beam scanning electron microscope (SEM, FEI Strata DB235). Bright-field imaging was conducted with TEM (JEOL JEM 2100) operated at 200 kV. X-ray photoelectron spectroscopy (Physical Electronics VersaProbe 5000) was carried out under ~$8 \times 10^{-9}$ Torr base pressure, with incident photon energy 1486.6 eV (Al $K_\alpha$ line) with the irradiation power 100 W over $100 \times 100$ $\mu m^2$. *In situ* XPS was collected from 250 °C to 400 °C with the step of 25 °C, from 400 °C to 600 °C with the step of 20 °C, and from 600 °C to 700 °C with the step of 25 °C. The heating rate was ~10 °C/min and acquisition time at each temperature was ~10 min.

Studies of the crystallization of the perovskite phase from the amorphous state on lattice-matched substrates (Figures 1(e) and 1(f)) are scarce. In order to determine the onset of crystallization of $BiFeO_3$ on (001)$SrTiO_3$ and (001)$LaAlO_3$, we used *in situ* X-ray diffraction (XRD) with a heating stage. Amorphous films grown by ALD initially contained an excess of Bi, which compensated for the bismuth oxide evaporation in the heating experiments. Epitaxial (001)$BiFeO_3$ starts to crystallize on $LaAlO_3$ at 350-400 °C and on $SrTiO_3$ at 450-500 °C. Figure 1 shows variable-temperature XRD patterns of the (001) peak for $BiFeO_3$ and the respective substrates. The films on the both substrates show a good degree of crystallinity above 450-500 °C. It is interesting to note that $BiFeO_3$ on $SrTiO_3$ demonstrates a sharp decrease of the (001) peak intensity above 640 °C, which gradually reaches the instrument noise level when the temperature approaches 760-780 °C. However, a similar drop of intensity, which is connected with the deterioration of the $BiFeO_3$ phase or its orientation, is absent

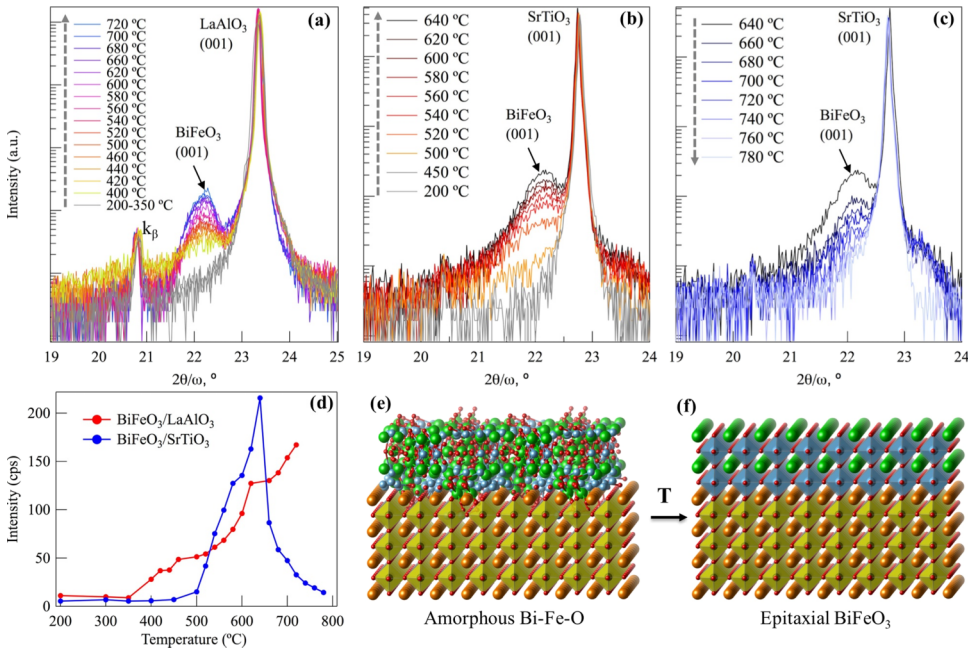


FIG. 1. X-ray diffraction patterns collected *in situ* during crystallization of amorphous Bi–Fe–O thin films initially grown by ALD. The appearance of the (001)$BiFeO_3$ during crystallization was observed for the (a) (001)$LaAlO_3$ and (b) and (c) (001)$SrTiO_3$ substrates. Dashed grey arrows show the direction of the temperature increase. In (c), the (001) reflection of $BiFeO_3$ started to decay with a further increase of temperature. (d) The change of the intensity of the (001) peak from $BiFeO_3$ during crystallization on different substrates. (e) and (f) The schematics of the crystallization process on a single-crystalline substrate.

for the film grown on $LaAlO_3$. One possible explanation of the smaller window of thermal stability of the $BiFeO_3$ film on $SrTiO_3$ can be its strained state as compared to the relaxed state of the film on $LaAlO_3$. Because epitaxial strain always destabilizes the film by introducing an additional positive term to the total Gibbs free energy, the perovskite film becomes unstable at lower temperature than in the case of the relaxed $BiFeO_3$. Another contributing factor is the smaller thickness of $BiFeO_3$ on $SrTiO_3$ (25 nm vs. 50 nm, estimated from the X-ray reflectivity), which could also lead to the faster disappearance of the (001) peak. In some cases, we observed the appearance of secondary phases (Figure 2(a), peaks at 32° and 35° related to the $Bi_{26-x}Fe_xO_{39}$ phase) during crystallization, which is inevitable when the initial composition is Bi > Fe. The presence of Bi-rich secondary phase in small quantities could also, in principle, postpone the onset of the perovskite phase decomposition. The appearance of these phases can be suppressed via short-time annealing of the stoichiometric amorphous film, as was demonstrated in our previous study[8] (if no long-time *in situ* study of annealing is needed).

Because the formation of phase-pure epitaxial $BiFeO_3$ via ALD and post-growth annealing has only been reported previously on $SrTiO_3$,[8] we performed detailed investigation of the epitaxial $BiFeO_3$ thin film on the $LaAlO_3$ substrate having a larger lattice mismatch. We note a small difference in the measured $c$ parameter of the $BiFeO_3$ film unit cell on different substrates: for $BiFeO_3/SrTiO_3$ $c$ = 4.0 Å (lattice strain $\epsilon$ = 0.9%) and for $BiFeO_3/LaAlO_3$ $c$ = 3.97 Å ($\epsilon$ = 0.1%). The theoretical in-plane lattice mismatches between bulk $BiFeO_3$ (pseudocubic $a$ = 3.965 Å) and the substrates are ~1.5% for $SrTiO_3$ and ~3.6% for $LaAlO_3$, respectively. The strain state of the films on $LaAlO_3$ and $SrTiO_3$ can also be observed in the reciprocal space maps (RSM) of the asymmetric (103) X-ray reflections (Figures 2(b) and 2(c)), where it is seen that the $BiFeO_3/SrTiO_3$ interface is in a coherently strained state.[8]

In contrast, the $BiFeO_3$ film on $LaAlO_3$ is relaxed (Figure 2(c)). Thus, the experimentally observed biaxial strain in the case of $BiFeO_3/SrTiO_3$ is larger than that of $BiFeO_3/LaAlO_3$, despite the opposite behavior expected theoretically. This has the following implications: *first*, it implies

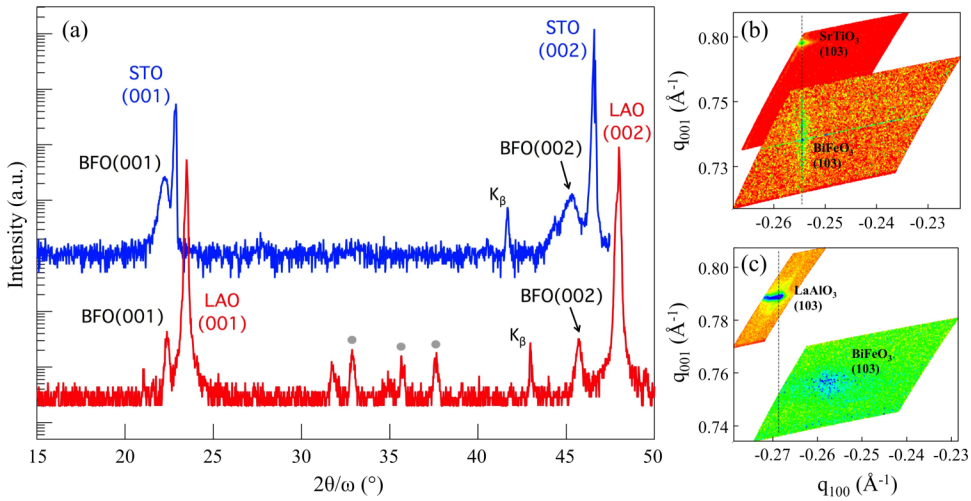


FIG. 2. (a) X-ray diffraction patterns of $BiFeO_3$ grown by ALD and post-growth annealing on (001)$SrTiO_3$ and (001)$LaAlO_3$. The peaks with grey dots are the reflections from the stage and are not related to the samples. (b) and (c) Reciprocal space maps of the (103) reflection of the (001)$BiFeO_3$ film grown on (001)$SrTiO_3$ and (001)$LaAlO_3$. BFO, STO, and LAO in the figure state for $BiFeO_3$, $SrTiO_3$, and $LaAlO_3$, respectively.

that the $BiFeO_3$ crystallization process leads to only partially strained films; *second*, a lower elastic strain of the film on a higher-lattice-mismatched substrate suggests that the epitaxially strained state of the ALD-grown and *ex situ* crystallized perovskite film can be obtained only on substrates with a relatively small lattice mismatch. Typically, thin films grown on (001)$LaAlO_3$ by PLD have a pseudomorphic layer with a tetragonal-like structure,[19] designated by strong (00*l*) reflections at ~19° and ~38° of 2$\theta$ (Cu $K_\alpha$ radiation). Absence of these reflections in our case (Figure 2(a)) suggests that annealing-induced strain relaxation does not preserve the strain coherency (the peaks with grey dots coming from the ceramic stage and are not related to the samples). Here, the epitaxialization via annealing suppresses the transition from rhombohedral to tetragonal-like $BiFeO_3$ and, instead, preserves the rhombohedral structure in ALD-grown and annealed $BiFeO_3$, apparently without sacrificing crystalline quality, as discussed below.

Transmission electron microscopy (TEM) imaging of the $BiFeO_3$ on $LaAlO_3$ was performed in order to determine the strain relaxation mechanism and compare the structure of the film to that grown on $SrTiO_3$. Due to the close matching of lattice parameters, $BiFeO_3$ grown on $SrTiO_3$ exhibits a dislocation-free interface.[8] However, during the crystallization of the $BiFeO_3$ on $LaAlO_3$, periodic misfit dislocations appear at the interface (Figures 3(a) and 3(b)). The dislocations are easily visible at low magnification owing to a strong bright-field contrast that changes periodically along the interface (supplementary material).[20] This contrast indicates substantial strain fields around the dislocation core which penetrates into the film for up to 5 nm. Selected-area electron diffraction (SAED) collected from the film+substrate region is shown in Figure 3(c), with $BiFeO_3$ reflections being closer to the (000) primary beam spot. Because the same SAED spots for both perovskites do not lie on the "vertical" line along the ⟨001⟩ direction (similarly to reciprocal space mapping (RSM)) but rather stay on the radial line, it is evident that the film is relaxed. High-resolution TEM of dislocations (Figures 3(d) and 3(e)) reveals visible lattice distortions in the region close to the interface.

In contrast to MOCVD, ALD is a low-temperature deposition technique and metal-organic precursors may be only partially oxidized in the film, which in turn can inhibit crystallization and change the phase content of the resulting film. To determine the oxidation states of elements in the as-grown amorphous films, we performed X-ray photoelectron spectroscopy (XPS) of individual oxides Bi–O and Fe–O as well as the complex oxide Bi–Fe–O thin films. Shown in Figures 4(a)-4(d) are the XPS results for Bi 4*f*, Fe 3*d*, and O 1*p* states (corrected using adventitious carbon). The position of the Bi peaks corresponds to its 3+ oxidation state. The Fe 3*d* spectra are different for Fe–O and Bi–Fe–O films, yet it is unclear what causes this difference in terms of the

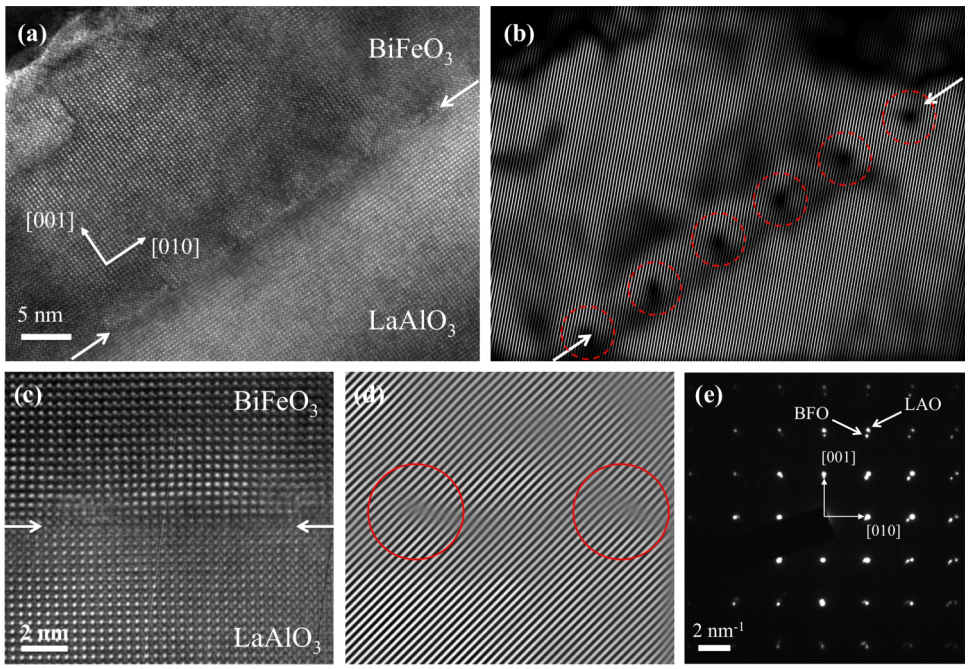


FIG. 3. (a) TEM image and (b) the corresponding Fourier-filtered image showing periodic misfit dislocations at the interface between the $BiFeO_3$ and $LaAlO_3$. (c) and (d) High-resolution image of the interface area and the dislocations showing that the dislocation cores are surrounded by defect-induced variation of lattice spacing. (e) Selected-area electron diffraction collected at the film-substrate interface indicates an overall unstrained state of $BiFeO_3$.

ALD chemistry. It is possible that Fe is underoxidized in Fe–O due to the use of sole ferrocene (no initial Fe–O bonds, $Fe^{2+}$ in ferrocene), while during the growth of the Bi–Fe–O film in each ALD supercycle $Bi(mmp)_3$ (6 Bi–O bonds) provides more oxygen-enriched layer for the Fe–O deposition. The oxygen peak has a small shoulder at higher energies for Bi–O, Fe–O, and Bi–Fe–O arising from residual carbon-oxygen bonds on the film surface. Interestingly, the oxygen peak in the Fe–O film is seen to shift to higher binding energies, implying a partial oxidation state of the oxygen $O^{-2+\delta}$ ($\delta > 0$).

To trace the evolution of the carbon content in the ALD-grown film, we performed XPS of the Bi–Fe–O film *in situ* under annealing. Carbon remains in the film up to ~500 °C and slowly disappears at a higher temperature (Figure 4). Interestingly, the amount of observable carbon seems

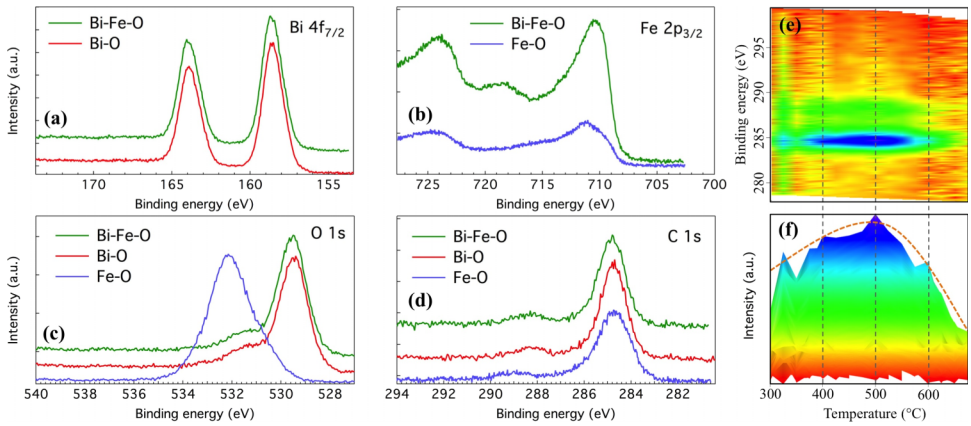


FIG. 4. (a)-(d) XPS of as-grown amorphous Bi–O, Fe–O, and Bi–Fe–O thin films. (e) and (f) *In situ* X-ray photoemission spectra collected for the carbon C 1*s* peak of the Bi–Fe–O film during annealing. The red dashed line is a guideline that reflects the carbon peak intensity change with temperature.

to increase when the temperature is varied from 300 to 500 °C, which points to the onset of considerable carbon diffusion from the bulk of the film to its surface. Because the measurements were carried out in an ultrahigh vacuum, it is likely that the annealing in an oxygen-rich atmosphere will make carbon evaporate (via oxidation) from the film surface at lower temperatures.

The *in situ* study of epitaxial crystallization of $BiFeO_3$ on the (001)$LaAlO_3$ and (001)$SrTiO_3$ substrates reveals the onset of crystallization to be substrate-dependent (above 350 °C and 450 °C, respectively). Tetragonality in ALD-grown and annealed $BiFeO_3$ on $LaAlO_3$ is suppressed, the film being relaxed and showing periodic misfit dislocations at the interface. The absence of the strained $BiFeO_3$ layer on $LaAlO_3$ implies that the *ex situ* annealing of ALD-grown perovskite films leads to the epitaxially strained state only in the case of a small lattice mismatch (less than ~1.5%). During the annealing process, Bi–Fe–O films showed the presence of carbon up to $T \sim 600$ °C, indicating the importance of carbon oxidation control during post-growth treatment. Our results demonstrate that the crystallization from the amorphous into the epitaxial film can act as the degree of freedom for engineering its epitaxial strain state. This is particularly important for enabling a low-temperature route to functional epitaxial films and realization of their strain-mediated polymorphism using atomic layer deposition.

We acknowledge the Drexel University core shared user facilities for access to XRD (NSF DMR 1040166), XPS (NSF CBET 0959361), FIB (NSF DMR 0722845), and TEM. Work at Drexel was supported by ONR under No. N00014-15-11-2170 and also by NSF under Nos. DMR 1124696 and IIP 1403463.

[1] J. H. Haeni, P. Irvin, W. Chang, R. Uecker, P. Reiche, Y. L. Li, S. Choudhury, W. Tian, M. E. Hawley, B. Craigo, A. K. Tagantsev, X. Q. Pan, S. K. Streiffer, L. Q. Chen, S. W. Kirchoefer, J. Levy, and D. G. Schlom, Nature **430**, 758 (2004).
[2] N. Tsvetkov, Q. Lu, Y. Chen, and B. Yildiz, ACS Nano **9**, 1613 (2015).
[3] K. J. Choi, M. Biegalski, Y. L. Li, A. Sharan, J. Schubert, R. Uecker, P. Reiche, Y. B. Chen, X. Q. Pan, V. Gopalan, L.-Q. Chen, D. G. Schlom, and C. B. Eom, Science **306**, 1005 (2004).
[4] J. H. Lee, L. Fang, E. Vlahos, X. Ke, Y. W. Jung, L. F. Kourkoutis, J.-W. Kim, P. J. Ryan, T. Heeg, M. Roeckerath, V. Goian, M. Bernhagen, R. Uecker, P. C. Hammel, K. M. Rabe, S. Kamba, J. Schubert, J. W. Freeland, D. A. Muller, C. J. Fennie, P. Schiffer, V. Gopalan, E. Johnston-Halperin, and D. G. Schlom, Nature **466**, 954 (2010).
[5] L. Marn, L. A. Rodrguez, C. Magen, E. Snoeck, R. Arras, I. Lucas, L. Morellon, P. A. Algarabel, J. M. De Teresa, and M. R. Ibarra, Nano Lett. **15**, 492 (2015).
[6] L. Martin, Y.-H. Chu, and R. Ramesh, Mater. Sci. Eng., R **68**, 89 (2010).
[7] D. G. Schlom, L.-Q. Chen, C.-B. Eom, K. M. Rabe, S. K. Streiffer, and J.-M. Triscone, Annu. Rev. Mater. Res. **37**, 589 (2007).
[8] A. R. Akbashev, G. Chen, and J. E. Spanier, Nano Lett. **14**, 44 (2013).
[9] N. Dix, R. Muralidharan, M. Varela, J. Fontcuberta, and F. Sanchez, Appl. Phys. Lett. **100**, 122905 (2012).
[10] R. R. Das, D. M. Kim, S. H. Baek, C. B. Eom, F. Zavaliche, S. Y. Yang, R. Ramesh, Y. B. Chen, X. Q. Pan, X. Ke, M. S. Rzchowski, and S. K. Streiffer, Appl. Phys. Lett. **88**, 242904 (2006).
[11] M. S. Kartavtseva, O. Y. Gorbenko, A. R. Kaul, A. R. Akbashev, T. V. Murzina, S. Fusil, A. Barthalamy, and F. Pailloux, Surf. Coat. Technol. **201**, 9149 (2007).
[12] J. Thery, C. Dubourdieu, T. Baron, C. Ternon, H. Roussel, and F. Pierre, Chem. Vap. Deposition **13**, 232 (2007).
[13] J. F. Ihlefeld, A. Kumar, V. Gopalan, D. G. Schlom, Y. B. Chen, X. Q. Pan, T. Heeg, J. Schubert, X. Ke, P. Schiffer, J. Orenstein, L. W. Martin, Y. H. Chu, and R. Ramesh, Appl. Phys. Lett. **91**, 071922 (2007).
[14] G. Catalan and J. F. Scott, Adv. Mater. **21**, 2463 (2009).
[15] V. Garcia and M. Bibes, Nat. Commun. **5**, 4289 (2014).
[16] D. Mazumdar, V. Shelke, M. Iliev, S. Jesse, A. Kumar, S. V. Kalinin, A. P. Baddorf, and A. Gupta, Nano Lett. **10**, 2555 (2010).
[17] B. Miao, R. Mahapatra, N. Wright, and A. Horsfall, J. Appl. Phys. **104**, 054510 (2008).
[18] Y. W. Kim, Y. Roh, J.-B. Yoo, and H. Kim, Thin Solid Films **515**, 2984 (2007).
[19] A. R. Damodaran, S. Lee, J. Karthik, S. MacLaren, and L. W. Martin, Phys. Rev. B **85**, 024113 (2012).
[20] See supplementary material at http://dx.doi.org/10.1063/1.4933064 for additional TEM image showing the periodic misfit dislocations at larger scale (low resolution).